# PROCGEN3D: LEARNING NEURAL PROCEDURAL GRAPHS FOR IMAGE-TO-3D RECONSTRUCTION

Xinyi Zhang<sup>1</sup>, Daoyi Gao<sup>1</sup>, Naiqi Li<sup>2</sup>, Angela Dai<sup>1</sup>

- <sup>1</sup> Technical University of Munich
- <sup>2</sup> Tsinghua University

xinyi.zhang@tum.de, daoyi.gao@tum.de, linaiqi.thu@gmail.com, angela.dai@tum.de

#### **ABSTRACT**

We introduce ProcGen3D, a new approach for 3D content creation by generating procedural graph abstractions of 3D objects, which can then be decoded into rich, complex 3D assets. Inspired by the prevalent use of procedural generators in production 3D applications, we propose a sequentialized, graph-based procedural graph representation for 3D assets. We use this to learn to approximate the landscape of a procedural generator for image-based 3D reconstruction. We employ edge-based tokenization to encode the procedural graphs, and train a transformer prior to predict the next token conditioned on an input RGB image. Crucially, to enable better alignment of our generated outputs to an input image, we incorporate Monte Carlo Tree Search (MCTS) guided sampling into our generation process, steering output procedural graphs towards more image-faithful reconstructions. Furthermore, this enables improved generalization on real-world input images, despite training only on synthetic data. Our approach is applicable across a variety of objects that can be synthesized with procedural generators. Extensive experiments on cacti, trees, and bridges show that our neural procedural graph generation outperforms both state-of-the-art generative 3D methods and domainspecific modeling techniques.

# 1 Introduction

Creating immersive 3D content is in significant demand, with widespread applications in industries such as film, gaming, mixed reality, architecture, robotics, and more. This has spurred on significant advances in generative 3D object modeling (Xiang et al., 2025; Chen et al., 2025), which have shown remarkable promise. However, these methods typically generate outputs as neural fields (Zhang et al., 2023; Xiang et al., 2025), points (Xie et al., 2021), or voxels (Ren et al., 2024b; Meng et al., 2025) that must then be converted into meshes for downstream applications, typically through Marching Cubes (Lorensen & Cline, 1998) – which results in over-tessellated meshes often lacking sharp geometry. In contrast, procedural modeling has long been a cornerstone in computer graphics, powering the creation of rich and diverse 3D content across many production applications (Müller et al., 2006; Parish & Müller, 2001; Raistrick et al., 2023). By encoding domain-specific rules and stochastic processes, they can synthesize highly complex structures (e.g., plants, terrain, or architectural designs) with remarkable realism while maintaining compact encodings. This offers a compelling alternative in generative 3D modeling, to synthesize lightweight, parametric representations that lead to complex, sophisticated geometric models as output.

Despite their expressive power, obtaining a desired procedural model based on specified user intent (e.g., image-based 3D reconstruction) remains a significant challenge – as the representation space is comparatively small while mixing continuous parameters with discrete choices. Additionally, procedural models typically involve stochastic sampling, which makes the relationship between input parameters and the final output nondifferentiable. This makes inverse procedural modeling through direct optimization very difficult.

To address these challenges, we propose to approximate the landscape of a procedural generator through a transformer-based neural network to encode a compact, abstract procedural graph repre-

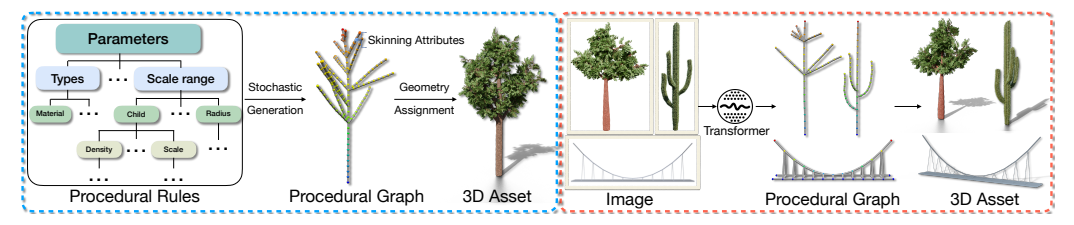


Figure 1: Left: procedural generators employ rule-based generation with stochastic sampling to produce abstract graph representations that are decoded into high-fidelity 3D assets through geometry and material assignment. Right: We propose to leverage such procedural graph representations, modeling their distribution with a transformer to enable high-fidelity image-to-3D reconstruction for various categories of procedurally generated objects (cacti, trees, bridges).

sentation for various 3D content, as shown in Fig. 1. Instead of storing only surface geometry, we abstract a 3D object into a graph whose nodes and edges capture its structural skeleton, together with spatial and geometric attributes. Such graphs are generated according to the underlying rules of a procedural generator, providing a concise and interpretable description of the object. The flexible and expressive graph representation allow our method capture the skeleton and attributes of 3D content in a way that is interpretable and structurally valid.

In contrast to 3D voxel, point, or neural field representations, using such a procedural generation basis enables capturing complex 3D content in a very compact form that can be decoded into rich 3D assets with complex, sharp detail that are directly suitable for downstream production applications.

Modeling such procedural graphs requires handling both their topological structure as well as dependencies between edges and attributes. Inspired by the success of autoregressive transformers (Vaswani et al., 2017) in language and multimodal modeling, we adopt a GPT-style transformer to learn procedural graph generation. Specifically, we sequentialize each graph into edge-based tokens, where each token encodes the spatial positions of its two endpoint vertices, their associated attributes, and the attributes of the edge. The transformer is then trained to autoregressively for next-token prediction.

We adopt this approach for image-based 3D reconstruction, conditioning our graph-based transformer on input image features. However, while this can produce output procedural graphs that can capture the overall structure of an object, this often struggles to reflect accurate fine-grained structural details of the input image (e.g., the precise growth direction of a cactus stem following the input image). This is partly due to the stochasticity of procedural generation and the vast combinatorial space of possible graphs. As a result, relying solely on autoregressive prediction from image features can lead to inconsistencies or loss of detail in the reconstructed graphs.

We thus propose to further integrate Monte Carlo Tree Search (MCTS) (Metropolis & Ulam, 1949; Browne et al., 2012) guided sampling into our inference process. We leverage MCTS to explore multiple candidate continuations of the token sequence, based on our learned transformer prior, aiming to balance exploration of new possibilities with exploitation of high-scoring predictions. By evaluating simulated sequences against the image condition and propagating the feedback through the search tree, MCTS refines the transformer's outputs and guides the generation toward procedural graphs that are both structurally consistent and more geometrically faithful to an input image. Additionally, our test-time search enables our approach, trained only on synthetic data where ground truth procedural graph information is available, to generalize to real images inputs. Our approach is versatile across various types of objects that can be modeled with procedural generators, which we demonstrate with experiments on three diverse categories: cacti, trees, and bridges.

The main contributions of our work are summarized as follows:

- We propose to learn a neural procedural graph-based representation for 3D assets, which enables modeling abstract procedural graphs that can decode to rich, complex 3D assets.
- Our approach enables neural inverse procedural modeling, conditioned on RGB images as input to predict procedural graph abstractions for various object categories.
- To improve adherence to the input images and better generalize to real image inputs, we introduce image guidance with Monte Carlo tree search (MCTS) during our generation process, enabling sampling from our learned prior while improving image consistency.

## 2 RELATED WORK

**Learning-Based 3D Object Generation.** Learning-based 3D generative methods have seen significant advances in recent years. Early approaches leveraged generative adversarial learning to train neural networks for unconditional 3D object synthesis (Wu et al., 2016; Gao et al., 2022). Following the success of denoising diffusion models for 2D image generation, diffusion modeling has been widely adopted for 3D generation of various representations, including voxels (Hui et al., 2022; Tang et al., 2023; Ren et al., 2024b; Meng et al., 2025), point clouds (Zhou et al., 2021; Luo & Hu, 2021), and neural field representations (Erkoç et al., 2023; Shue et al., 2023; Xiang et al., 2025). These methods have shown remarkable potential in synthesizing visually compelling 3D objects; however, they rely on Marching Cubes (Lorensen & Cline, 1998) post-processing to convert outputs into meshes for downstream applications, resulting in over-tessellated and over-smoothed geometric outputs. Similarly, the success of autoregressive transformers in natural language modeling has also inspired the use of GPT-style transformers for mesh generation (Siddiqui et al., 2024; Chen et al., 2024). These methods can produce much more compact, sharper mesh outputs, but are limited in sequence context to low face count outputs. Our approach also leverages GPT-style autoregressive transformers, but rather than operate on lengthy mesh sequences, we focus on modeling procedural graph representations. This representation is inherently more compact and expressive, allowing later decoding into sophisticated, high-fidelity 3D assets.

**Image-to-3D Generation.** For many downstream tasks, user input to control the generation process plays a key role. In particular, input RGB images provide a simple and very accessible way to guide 3D object generation. Various methods have been proposed to leverage diffusion to generate neural fields from input images, representing output 3D shape geometry (Zhang et al., 2023) and 3D radiance fields (Müller et al., 2023; Liu et al., 2023; Oian et al., 2023; Long et al., 2024; Xiang et al., 2025), along with accelerated generation through transformer training (Hong et al., 2023). Tree-D Fusion (Lee et al., 2024) also introduces a domain-specific model leveraging diffusion priors, in order to synthesize trees from image inputs. A more prevalent approach has been to leverage large shape databases for training; for instance, TRELLIS (Xiang et al., 2025) employs latent flow matching to show remarkable 3D shape synthesis results from images. However, these methods all rely on Marching Cubes-style post-processing to obtain mesh outputs, which can introduce noise and oversmoothing in the output geometry. Furthermore, while such diffusion-based models can generated 3D shapes from an image, their outputs are primarily guided by a learned prior, and may not remain consistent with the input image, especially in the local structure. In contrast, we employ not only a compact, procedural graph representation, but moreover, we propose a MCTS-guided test-time search to synthesize outputs that align well with the image input.

Inverse Procedural Modeling. Though procedural modeling (Müller et al., 2006; Parish & Müller, 2001; Raistrick et al., 2023) has been widely used to generate high-quality 3D assets, the inverse problem – recovering procedural representations from observed data – remains highly challenging due to the combinatorial search space and the nondifferentiable nature of many procedural generators. Early work on inverse procedural modeling primarily focused on recovering procedural rules through optimization and grammar induction of one specific category of objects, such as trees (Št'ava et al., 2010) or buildings (Wu et al., 2013). These methods typically assume a predefined grammar, such as L-systems or split grammars, and attempt to infer rule parameters or production rules that best explained the observed data. Approaches in this category often relied on handcrafted heuristics, probabilistic inference, or search-based strategies to align generated procedural structures with target observations (Martinovic & Van Gool, 2013). While effective for relatively constrained single domains such as plants or architectural facades, they tend to be sensitive and struggle to scale to highly complex or noisy real-world data.

Recently, several learning-based approaches have been proposed to overcome limitations of purely grammar-driven methods. These methods leverage neural networks to regress procedural parameters directly from input observations or to approximate procedural generators with differentiable surrogates, enabling gradient-based optimization (Plocharski et al., 2024). Generation-based approaches have also been explored, directly generating procedural parameters from images using conditional diffusion models (Zhao et al., 2025). While effective, these methods are primarily suited for objects with relatively simple structures. In contrast, our method targets more complex categories by recovering full procedural graphs that explicitly capture both structural skeleton and geometric attributes. We further demonstrate its versatility across diverse output types, including cacti, trees, and bridges.

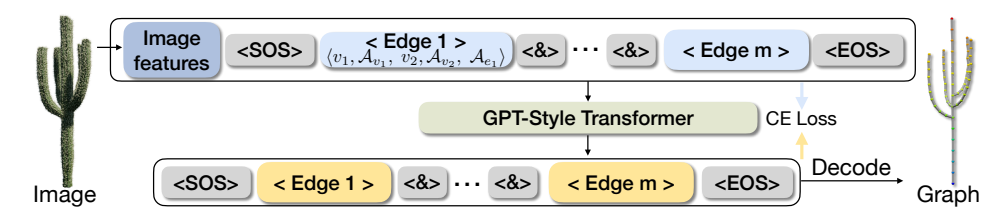


Figure 2: Overview of our graph-based transformer. A procedural graph is tokenized into a sequence of edge-based tokens, where each token encodes the positions and attributes of its two endpoint vertices as well as the attributes of the edge itself. The transformer autoregressively predicts tokens conditioned on image features, enabling reconstruction of the underlying procedural graph.

## 3 Method

We introduce our procedural graph-based 3D representation  $\mathcal{G}$ , which encodes a 3D object as a set of nodes and edges, enriched with geometric and semantic attributes. We then use this representation for image to 3D reconstruction by training a transformer model  $\mathcal{T}$  to predict the underlying procedural graph from an RGB image observation. To facilitate faithful reconstructions to the input image, we further introduce MCTS-guided sampling of  $\mathcal{T}$  at test time.

#### 3.1 PROCEDURAL GRAPH REPRESENTATION

Inverse procedural modeling is often formulated as recovering the initial parameters of a procedural generator; however, the non-differentiable stochastic sampling during generation makes this very difficult to optimize directly. Instead, we propose to approximate the landscape of procedural generation by training a transformer on an intermediate procedural graph representation G.

The graph  $\mathcal G$  encodes the procedural information, capturing both structural skeleton information along with spatial and geometric attributes in its nodes and edges. This enables modeling a tractable and expressive basis for modeling and reconstructing complex 3D assets from image observations.  $\mathcal G$  is then represented as a graph with n nodes and m edges, where each node and edge is associated with a set of attributes:

$$\mathcal{G} = (V, E, \mathcal{A}_V, \mathcal{A}_E) \tag{1}$$

where  $V = \{v_1, \dots, v_n\}$  denotes the set of nodes,  $E = \{e_1, \dots, e_m\} \subseteq V \times V$  is the set of edges,  $A_V$  the node attributes (e.g., class label, radius), and  $A_E$  the edge attributes (e.g., length, force, semantic type, etc.).

From a graph  $\mathcal{G}$ , the procedural generator can then assign detailed geometry along with material and texture to the mesh surface, producing watertight, manifold meshes with clean topology, which is difficult to achieve with voxel or neural field based 3D representations. With this compact representation, a complex tree mesh with more than 10 million faces can be abstracted as a graph with only a few hundred nodes, greatly reducing both computation and storage costs.

## 3.2 MODELING PROCEDURAL GRAPHS WITH A TRANSFORMER

Inspired by the success of multimodal large language models, we use an autoregressive transformer to model procedural graphs. We first convert each graph into a sequence of edge-based tokens.

Given a graph  $\mathcal{G}$  with m edges, we treat each edge as a unit for tokenization. For an edge connecting vertices  $v_a$  and  $v_b$ , we represent its token as

$$\tau(e_i) = (v_a, \mathcal{A}_{v_a}, v_b, \mathcal{A}_{v_b}, \mathcal{A}_{e_i}), \tag{2}$$

where  $A_{v_a}$  and  $A_{v_b}$  denote the attribute sets of the two endpoint vertices, and  $A_{e_i}$  represents the attributes associated with the edge itself. Note that for simplicity, as we will describe our method in terms of tokenized edges, we will use  $e_i$  to denote  $\tau(e_i)$ .

For the entire graph, we tokenize all edges in a predefined spatial traversal order. Specifically, we use a depth-first search (DFS) order for plant-like structures and a breadth-first search (BFS) order for architectures such as bridges. Between consecutive edge tokens, we insert a special split token

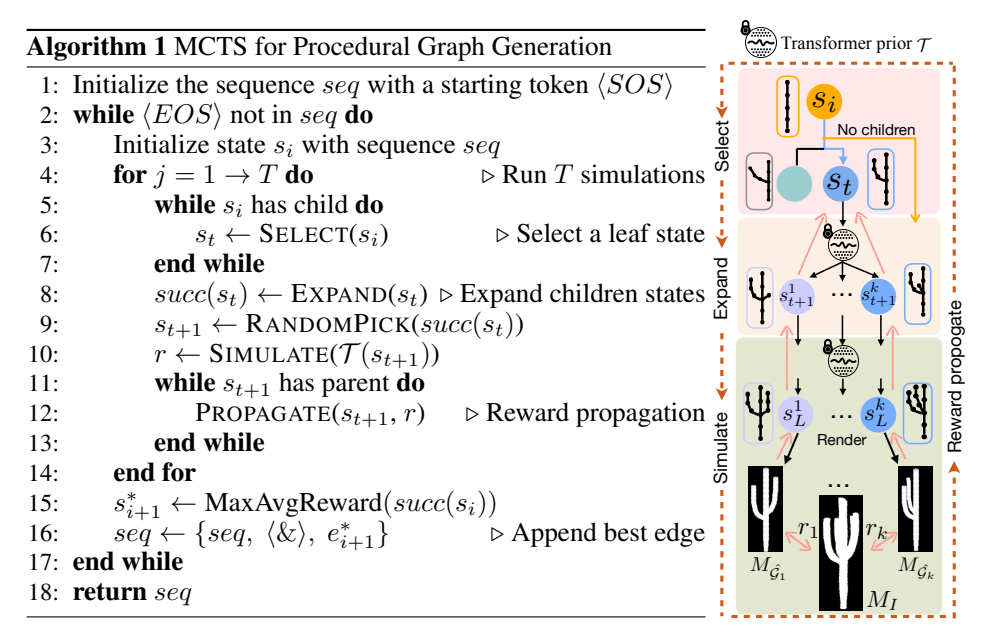


Figure 3: Overview of our MCTS-guided search to reconstruct a procedural graph that well-aligns to the input image condition.

```
\langle \& \rangle to explicitly indicate edge boundaries, producing our final tokenized sequence as: \mathcal{S}(\mathcal{G}) = \{e_1, \langle \& \rangle, e_2, \langle \& \rangle, \dots, e_m\}.
```

Similar to works leveraging transformers for mesh triangle generation (Chen et al., 2024; Tang et al., 2024), we directly use the discretized coordinates of our graph vertices and the class indices of attributes as the token indices. A GPT-style transformer  $\mathcal{T}$  is then trained autoregressively to predict tokens sequentially with a Cross Entropy loss, conditioned on image features z extracted from the input RGB image I by a pretrained image encoder (Ranzinger et al., 2024)  $z = \phi(I)$ .

## 3.3 AUTOREGRESSIVE GENERATION WITH MCTS-GUIDED SAMPLING

During inference, we encode an input image I into its features  $z=\phi(I)$ , and feed z into the transformer  $\mathcal{T}$ , which autoregressively generates an output token sequence representing a procedural graph  $\mathcal{G}$ . While conditioning solely on z allows the model to capture the overall structure of the object, relying soley on the learned prior can lose accuracy in aligning to finer-grained image details. To address this, we introduce a Monte Carlo Tree Search (MCTS) guided sampling into our generation process to refine the synthesized token sequence to better align with the image condition. For alignment guidance, we extract from I its mask  $M_I$  (e.g., with SAM (Kirillov et al., 2023; Ren et al., 2024a)). We then compare  $M_I$  with our rendered silhouette  $M_{\hat{\mathcal{G}}}$  of the currently generated  $\hat{\mathcal{G}}$ .

MCTS enables effectively analyzing the most promising choices for the next potential edge in  $\mathcal{G}$  by expanding a search tree through random sampling of the search space, based on our learned prior from  $\mathcal{T}$ . More specifically, we treat a single edge e comprising p tokens as the minimal search unit and apply MCTS to explore edge candidates that best align with the image condition I.

Our MCTS procedure adopts the standard four-stage procedure: **selection**, **expansion**, **simulation**, and **reward propagation**<sup>1</sup>, which are repeated iteratively.

Formally, we define states and successor relation of MCTS as follows:

- $\circ$  States S: each state  $s_i \doteq \{e_1, \ \langle \& \rangle, \ e_2, \ \langle \& \rangle, \ \dots, \ e_i\} \in S$  is a partial graph.
- $\circ$  The child state relation is defined by the successor function:  $s' \in succ(s_i)$ , if there exists some  $e_{i+1}$  s.t.  $s' \doteq \{e_1, \langle \& \rangle, e_2, \langle \& \rangle, \ldots, e_i, \langle \& \rangle, e_{i+1}\}$ .

<sup>&</sup>lt;sup>1</sup>Referred to as backpropagation in standard MCTS; we use the term reward propagation here to distinguish it from gradient backpropagation.

**Selection.** Starting from a sequence of previously generated partial graph  $seq = s_i$ , our goal is to identify a promising leaf state  $s_t^*$  for simulating future performance. Note that at the beginning of the search,  $s_i$  has no children, and so will be directly selected as the target leaf for expansion. As iterations proceed, however, the number of child states grows exponentially.

While a purely greedy search over all possible leaf states could in principle yield good results, the vast search space makes it computationally infeasible. On the other hand, focusing only on states with highest current scores risks getting trapped in local minima due to limited exploration.

To balance exploration and exploitation, we recursively select promising child states  $\{s_{i+1}^*, s_{i+2}^*, ...\}$  according to an Upper Confidence Bound (UCB) criterion until a leaf state  $s_t^*$  is reached,

$$s_{i+1}^* = \arg\max_{s_{i+1}} \left( Q(s_i, s_{i+1}) + c\sqrt{\frac{\log N(s_i)}{1 + N(s_i, s_{i+1})}} \right), \tag{3}$$

where  $Q(s_i, s_{i+1})$  is the average reward of choosing candidate child state  $s_{i+1} \in succ(s_i)$ ,  $N(s_i)$  and  $N(s_i, s_{i+1})$  are the visit counts of state  $s_i$  and state  $s_{i+1}$ , and c is an exploration constant.

**Expansion.** At a leaf state  $s_t$ , new candidate child states  $succ(s_t)$  are added to the search tree by predicting the next possible edges. Given the predicted logits  $\ell$  from the transformer prior, we sequentially sample p tokens to form an edge candidate and collect a set of candidates  $\mathcal{E} = \{e_{t+1}^1,...,e_{t+1}^k\}$  as potential continuations of the sequence, forming a set of new child states  $succ(s_t) = \{e_{1:t}, \langle \& \rangle, e_{t+1} \mid e_{t+1} \in \mathcal{E}\}.$ 

Simulation & Reward Propagation. After expanding new edges, we simulate their subsequent performance by using the transformer  $\mathcal{T}$  to autoregressively generate future tokens up to a predefined length L (e.g., the next 10 edges):  $\mathcal{T}(e_{t+1:L} \mid \mathbf{z}) = \prod_{l=t+1}^{L} \mathcal{T}(e_l \mid e_{< l}, \mathbf{z})$ .

For each simulation, the quality of the generated sequence is evaluated against the image condition I. Specifically, edges are represented as cylinders and rendered in real time to obtain a mask  $M_{\hat{\mathcal{G}}}$  of the generated graph  $\hat{\mathcal{G}}=\{e_{1:L}\}$ . The overlap between  $M_{\hat{\mathcal{G}}}$  and the mask  $M_I$  extracted from the input I is then computed to yield a reward score r:

$$r = \lambda \cdot \frac{|M_I \cap M_{\hat{\mathcal{G}}}|}{|M_{\hat{\mathcal{G}}}|} + (1 - \lambda) \cdot \frac{|M_I \cap M_{\hat{\mathcal{G}}}|}{|M_I|},\tag{4}$$

where  $\lambda \in [0,1]$  balances the two overlap ratios. r is then propagated back through all parent states  $\{s_{i+1},...,s_t\}$  to update their average reward.

After completing all simulations, the child state of the root state with the highest average reward  $s_{i+1}^*$  is selected as the best candidate, and its corresponding edge sequence  $\{e_{1:i+1}\}$  becomes the new root state for the next iteration. By iteratively applying these four steps, MCTS effectively guides sampling to edge sequences representing procedural graphs more consistent with the image.

# 4 EXPERIMENTS

In our experimental results, we report quantitative and qualitative evaluations on synthetic procedurally generated data (as described below), where ground truth data is available for evaluation. We further demonstrate the applicability of ProcGen3D to real images, where no ground truth exists but qualitative results highlight our generalization ability.

**Dataset.** We construct a dataset using procedural generators for both natural and man-made structures. For natural categories, we use Infinigen (Raistrick et al., 2023) to generate diverse instances of cacti and trees. For trees, this encompasses both standard and pine trees, and we consider two evaluation settings: (i) branches only, which allows accurate assessment of structural alignment, and (ii) with foliage (leafy), which introduces significant occlusion and in a more challenging reconstruction scenario. For man-made structures, we adopt a Combinatorial Equilibrium Modeling (CEM) (Ohlbrock & D'Acunto, 2020) procedural generator to produce bridges.

Each generated object is represented by its procedural graph and paired rendered RGB images. For each category, we generate 10,000 samples (9500/100/400 train/val/test). We collect different sets

of attributes depending on the data category:

- $\circ$  Cactus: node attributes include (x, y, z) coordinates and branch radius.
- $\circ$  Tree: node attributes include (x, y, z) coordinates.
- $\circ$  Bridge: node attributes include (x, y, z) coordinates and semantic type, while edge attributes include the sign of force, semantic type, and CEM type.

Note that these procedural graphs can then be fed back into the corresponding original procedural generators to produce high-fidelity 3D assets.

**Implementation Details.** We adopt OPT-350M (Zhang et al., 2022) as our transformer architecture, and the Radio (Ranzinger et al., 2024) pretrained image encoder. For token prediction, we discretize continuous attributes (e.g., coordinates, radii) into 128 classes. For n-class categorical attributes, we assign token indices in [128, 128 + n) to avoid overlap with continuous attributes. During the transformer embedding stage, discretized coordinates and radii are embedded into 1024-dimensional feature vectors. For tokens representing semantic attributes, we use a pretrained CLIP encoder (Radford et al., 2021) to embed their text labels, followed by a linear projection into a 1024-dimensional space. All token embeddings are then concatenated in their original order to form the input sequence to the transformer. Our model is trained with one A6000 GPU for one day.

## 4.1 IMAGE TO 3D RECONSTRUCTION

**Baselines.** We compare our image to 3D reconstruction results with state-of-the-art image to 3D generative methods TRELLIS (Xiang et al., 2025) and Wonder3D (Long et al., 2024). We further compare with the domain-specific method TreeDFusion (Lee et al., 2024) on the leafy tree category.

**Evaluation metrics.** Following prior work (Lee et al., 2024), we evaluate both 3D and 2D metrics: 1) Chamfer Distance between point clouds sampled from ground-truth meshes and reconstructed meshes (direct outputs from baselines; reconstructed from generated graphs via the corresponding procedural generator for our method), 2) LPIPS and 3) CLIP similarity between the input RGB images and renderings of the reconstructions.

As shown in Tab. 1, our method outperforms all baselines across all categories, demonstrating superior geometric accuracy, perceptual fidelity, and semantic alignment with the input images. Qualitative results in Fig. 4 further show that our reconstructions better align with input images. In particular, Wonder3D often fails to reconstruct fine-grained structures (e.g., dense or thin elements), while TRELLIS can capture the overall structure but struggles with local geometric fidelity, leading to distorted or physically implausible details such as broken branches and bridge cables. In contrast, our procedural graph representation inherently encourages structural correctness during reconstruction. This allows ProcGen3D to preserve both global structure and fine-grained details, producing reconstructions that are much more consistent in both structure and geometry.

## 4.2 ABLATIONS

To evaluate the effectiveness of our representation in capturing structural correctness, we conduct ablation studies focusing on the impact of different input modalities (mask vs. RGB), tokenization ordering (DFS vs. BFS), and our use of MCTS guided sampling.

**Effect of input image modality and tokenization order** We first study the influence of different input modalities and tokenization strategies on reconstruction quality. We consider only using extracted image masks as input rather than RGB along with extracted masks. As shown in Tab. 2, the RGB inputs tend to provide more information (particularly regarding occlusions), leading to better performance. We also compare depth-first search (DFS) and breadth-first search (BFS) orders for graph tokenization. While both orders achieve similar levels of topological consistency, DFS exhibits a clear advantage in preserving spatial fidelity.

**Effect of MCTS guided sampling** To assess the effectiveness of our MCTS-guided sampling in capturing accurate fine-grained local detail, we compare to a baseline variant of our approach conditioned solely on RGB images without MCTS. As shown in Tab. 3, incorporating MCTS consistently improves reconstruction quality across all categories. These improvements are particularly pronounced in challenging cases with fine-grained details, where direct autoregressive generation often fails to capture local geometry accurately. However, in the case of leafy trees, the mask becomes

Table 1: Comparison with TRELLIS (Xiang et al., 2025), Wonder3D (Long et al., 2024) and TreeD-Fusion (Lee et al., 2024). Our approach achieves superior performance across all categories, in both 3D and 2D metrics.

Category	Method	CD↓	LPIPS ↓	CLIP-Sim ↑
	TRELLIS	0.0456	0.195	0.9222
Cactus	Wonder3D	0.0375	0.141	0.9029
	Ours	0.0297	0.097	0.9268
	TRELLIS	0.0459	0.158	0.9644
Tree	Wonder3D	0.0479	0.212	0.9013
	Ours	0.0265	0.081	0.9769
	TRELLIS	0.0775	0.199	0.9348
Leafy Tree	Wonder3D	0.0745	0.214	0.8748
	TreeDFusion	0.0991	0.356	0.8543
	Ours	0.0648	0.168	0.9493
	TRELLIS	0.0508	0.204	0.9496
Pine tree	Wonder3D	0.0599	0.254	0.8834
	Ours	0.0302	0.079	0.9680
	TRELLIS	0.0363	0.156	0.9175
Bridge	Wonder3D	0.1097	0.302	0.7763
_	Ours	0.0141	0.052	0.9820

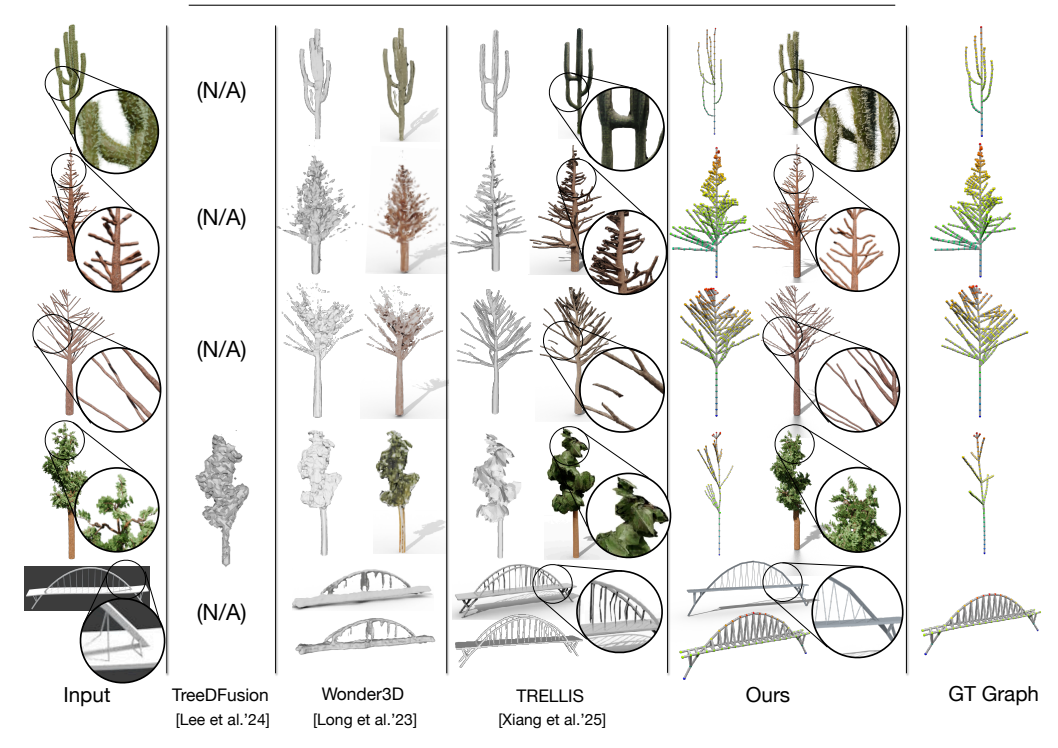


Figure 4: Qualitative comparison with state-of-the-art 3D generative models TRELLIS and Wonder3D. ProcGen3D achieves higher-fidelity reconstructions on all categories.

heavily expanded due to occlusion, which can cause MCTS to generate additional branches, leading to a slight drop in topological similarity. For real images, as shown in Sec. 4.3, our MCTS guided sampling improves over conditional generation only on leafy trees, as conditional generation suffers more from a larger domain gap.

# 4.3 GENERALIZATION TO REAL-WORLD IMAGES

We further test our method's ability to generalize to real-world photos collected from the internet. We employ Grounded-SAM (Ren et al., 2024a) to extract the mask of the main object, and use the masked image as input. As shown in Fig. 5, while baselines can capture overall structures of

Table 2: Ablation study of our design choices on the tree category. The results show that both incorporating RGB information and adopting an appropriate tokenization order significantly improve structural consistency and geometric fidelity in reconstruction.

Categroy	Setting	CD↓	Topo-Sim ↑	LPIPS ↓	CLIP-Sim↑
	mask_input	0.0485	0.958	0.166	0.9319
Tree	rgb_input	0.0265	0.971	0.081	0.9769
TICC	BFS_order	0.0336	0.972	0.137	0.9701
	DFS_order	0.0265	0.971	0.081	0.9769

Table 3: Ablation study of our MCTS guided sampling vs. image-conditioned generation only. The results demonstrate that incorporating MCTS significantly improves consistency with the inputs.

Category	Method	CD↓	Topo-Sim ↑	LPIPS ↓	CLIP-Sim↑
Cactus	w/o MCTS	0.0311	0.985	0.108	0.9268
Cactus	w MCTS (Ours)	0.0297	0.987	0.097	0.9268
Tree	w/o MCTS	0.0312	0.970	0.116	0.9533
1166	w MCTS (Ours)	0.0265	0.971	0.081	0.9769
I and Tues	w/o MCTS	0.0653	0.962	0.152	0.9424
Leafy Tree	w MCTS (Ours)	0.0648	0.948	0.168	0.9493
Pine tree	w/o MCTS	0.0313	0.980	0.091	0.9673
rine nee	w MCTS (Ours)	0.0302	0.983	0.079	0.9677
Bridge	w/o MCTS	0.0164	0.996	0.058	0.9785
	w MCTS (Ours)	0.0141	0.998	0.052	0.9820

the target objects, they struggle to recover fine-grained details. In contrast, our method produces more physically plausible and topologically similar structures. Furthermore, incorporating MCTS guidance improves the alignment between the generated graphs and the target image, yielding more consistent reconstructions than our variant without MCTS.

## 5 Conclusion

We have presented ProcGen3D, a new approach for reconstructing 3D objects from RGB images by synthesizing compact procedural graph abstractions, which then can be decoded with a procedural generator into high-fidelity 3D assets. Our method trains a transformer to approximate the land-scape of the procedural generator in the procedural graph space, using an edge-based tokenization strategy to represent procedural graphs as sequences. Unlike existing methods that rely solely on a learned prior for image-to-3D reconstruction, we incorporate an MCTS-guided search over the transformer prior, enabling reconstructions that more faithfully capture local structures of the input image. This yields higher-fidelity synthesis, and we hope this highlights the potential of alternative representations in 3D content creation.

**Acknowledgments.** This project was supported by the ERC Starting Grant SpatialSem (101076253) and the TUM Georg Nemetschek Institute Artificial Intelligence for the Built World.

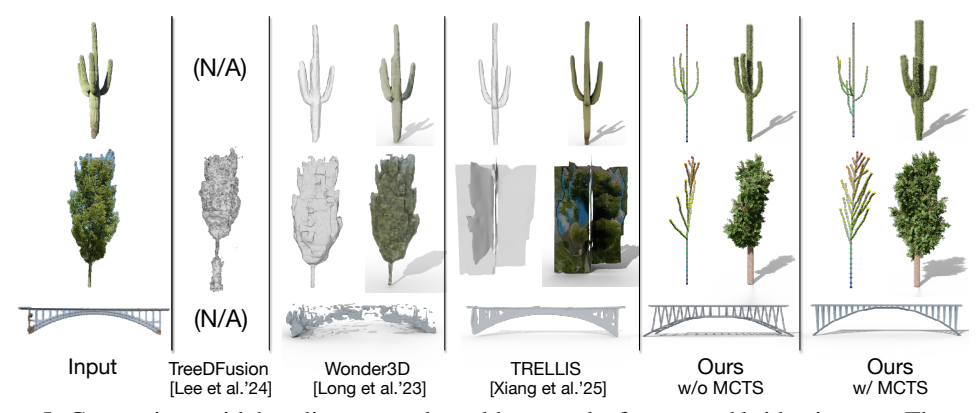


Figure 5: Comparison with baselines on real-world cactus, leafy tree, and bridge images. The results demonstrate that our model generalizes effectively to real-world data, despite being trained only on synthetic data.

## REFERENCES

- Cameron B Browne, Edward Powley, Daniel Whitehouse, Simon M Lucas, Peter I Cowling, Philipp Rohlfshagen, Stephen Tavener, Diego Perez, Spyridon Samothrakis, and Simon Colton. A survey of monte carlo tree search methods. *IEEE Transactions on Computational Intelligence and AI in games*, 4(1):1–43, 2012.
- Yiwen Chen, Yikai Wang, Yihao Luo, Zhengyi Wang, Zilong Chen, Jun Zhu, Chi Zhang, and Guosheng Lin. Meshanything v2: Artist-created mesh generation with adjacent mesh tokenization. *arXiv* preprint arXiv:2408.02555, 2024.
- Zhaoxi Chen, Jiaxiang Tang, Yuhao Dong, Ziang Cao, Fangzhou Hong, Yushi Lan, Tengfei Wang, Haozhe Xie, Tong Wu, Shunsuke Saito, et al. 3dtopia-xl: Scaling high-quality 3d asset generation via primitive diffusion. In *Proceedings of the Computer Vision and Pattern Recognition Conference*, pp. 26576–26586, 2025.
- Ziya Erkoç, Fangchang Ma, Qi Shan, Matthias Nießner, and Angela Dai. Hyperdiffusion: Generating implicit neural fields with weight-space diffusion. In *Proceedings of the IEEE/CVF international conference on computer vision*, pp. 14300–14310, 2023.
- Jun Gao, Tianchang Shen, Zian Wang, Wenzheng Chen, Kangxue Yin, Daiqing Li, Or Litany, Zan Gojcic, and Sanja Fidler. Get3d: A generative model of high quality 3d textured shapes learned from images. *Advances in neural information processing systems*, 35:31841–31854, 2022.
- Yicong Hong, Kai Zhang, Jiuxiang Gu, Sai Bi, Yang Zhou, Difan Liu, Feng Liu, Kalyan Sunkavalli, Trung Bui, and Hao Tan. Lrm: Large reconstruction model for single image to 3d. arXiv preprint arXiv:2311.04400, 2023.
- Ka-Hei Hui, Ruihui Li, Jingyu Hu, and Chi-Wing Fu. Neural wavelet-domain diffusion for 3d shape generation. In *SIGGRAPH Asia 2022 conference papers*, pp. 1–9, 2022.
- Alexander Kirillov, Eric Mintun, Nikhila Ravi, Hanzi Mao, Chloe Rolland, Laura Gustafson, Tete Xiao, Spencer Whitehead, Alexander C Berg, Wan-Yen Lo, et al. Segment anything. In *Proceedings of the IEEE/CVF international conference on computer vision*, pp. 4015–4026, 2023.
- Jae Joong Lee, Bosheng Li, Sara Beery, Jonathan Huang, Songlin Fei, Raymond A Yeh, and Bedrich Benes. Tree-d fusion: Simulation-ready tree dataset from single images with diffusion priors. In *European Conference on Computer Vision*, pp. 439–460. Springer, 2024.
- Ruoshi Liu, Rundi Wu, Basile Van Hoorick, Pavel Tokmakov, Sergey Zakharov, and Carl Vondrick. Zero-1-to-3: Zero-shot one image to 3d object. In *Proceedings of the IEEE/CVF international conference on computer vision*, pp. 9298–9309, 2023.
- Xiaoxiao Long, Yuan-Chen Guo, Cheng Lin, Yuan Liu, Zhiyang Dou, Lingjie Liu, Yuexin Ma, Song-Hai Zhang, Marc Habermann, Christian Theobalt, et al. Wonder3d: Single image to 3d using cross-domain diffusion. In *Proceedings of the IEEE/CVF conference on computer vision and pattern recognition*, pp. 9970–9980, 2024.
- William E Lorensen and Harvey E Cline. Marching cubes: A high resolution 3d surface construction algorithm. In *Seminal graphics: pioneering efforts that shaped the field*, pp. 347–353. 1998.
- Shitong Luo and Wei Hu. Diffusion probabilistic models for 3d point cloud generation. In *Proceedings of the IEEE/CVF conference on computer vision and pattern recognition*, pp. 2837–2845, 2021.
- Andelo Martinovic and Luc Van Gool. Bayesian grammar learning for inverse procedural modeling. In *Proceedings of the IEEE Conference on Computer Vision and Pattern Recognition*, pp. 201–208, 2013.
- Quan Meng, Lei Li, Matthias Nießner, and Angela Dai. Lt3sd: Latent trees for 3d scene diffusion. In *Proc. Computer Vision and Pattern Recognition (CVPR), IEEE*, 2025.
- Nicholas Metropolis and Stanislaw Ulam. The monte carlo method. *Journal of the American statistical association*, 44(247):335–341, 1949.

- Norman Müller, Yawar Siddiqui, Lorenzo Porzi, Samuel Rota Bulo, Peter Kontschieder, and Matthias Nießner. Diffrf: Rendering-guided 3d radiance field diffusion. In *Proceedings of the IEEE/CVF Conference on Computer Vision and Pattern Recognition*, pp. 4328–4338, 2023.
- Pascal Müller, Peter Wonka, Simon Haegler, Andreas Ulmer, and Luc Van Gool. Procedural modeling of buildings. In *ACM SIGGRAPH 2006 Papers*, pp. 614–623. 2006.
- Patrick Ole Ohlbrock and Pierluigi D'Acunto. A computer-aided approach to equilibrium design based on graphic statics and combinatorial variations. Computer-Aided Design, 121:102802, 2020.
- Yoav IH Parish and Pascal Müller. Procedural modeling of cities. In *Proceedings of the 28th annual conference on Computer graphics and interactive techniques*, pp. 301–308, 2001.
- Aleksander Plocharski, Jan Swidzinski, Joanna Porter-Sobieraj, and Przemyslaw Musialski. Façaid: A transformer model for neuro-symbolic facade reconstruction. In *SIGGRAPH Asia 2024 Conference Papers*, pp. 1–11, 2024.
- Guocheng Qian, Jinjie Mai, Abdullah Hamdi, Jian Ren, Aliaksandr Siarohin, Bing Li, Hsin-Ying Lee, Ivan Skorokhodov, Peter Wonka, Sergey Tulyakov, et al. Magic123: One image to high-quality 3d object generation using both 2d and 3d diffusion priors. *arXiv preprint arXiv:2306.17843*, 2023.
- Alec Radford, Jong Wook Kim, Chris Hallacy, Aditya Ramesh, Gabriel Goh, Sandhini Agarwal, Girish Sastry, Amanda Askell, Pamela Mishkin, Jack Clark, et al. Learning transferable visual models from natural language supervision. In *International conference on machine learning*, pp. 8748–8763. PmLR, 2021.
- Alexander Raistrick, Lahav Lipson, Zeyu Ma, Lingjie Mei, Mingzhe Wang, Yiming Zuo, Karhan Kayan, Hongyu Wen, Beining Han, Yihan Wang, et al. Infinite photorealistic worlds using procedural generation. In *Proceedings of the IEEE/CVF conference on computer vision and pattern recognition*, pp. 12630–12641, 2023.
- Mike Ranzinger, Greg Heinrich, Jan Kautz, and Pavlo Molchanov. Am-radio: Agglomerative vision foundation model reduce all domains into one. In *Proceedings of the IEEE/CVF conference on computer vision and pattern recognition*, pp. 12490–12500, 2024.
- Tianhe Ren, Shilong Liu, Ailing Zeng, Jing Lin, Kunchang Li, He Cao, Jiayu Chen, Xinyu Huang, Yukang Chen, Feng Yan, et al. Grounded sam: Assembling open-world models for diverse visual tasks. *arXiv preprint arXiv:2401.14159*, 2024a.
- Xuanchi Ren, Jiahui Huang, Xiaohui Zeng, Ken Museth, Sanja Fidler, and Francis Williams. Xcube: Large-scale 3d generative modeling using sparse voxel hierarchies. In *Proceedings of the IEEE/CVF conference on computer vision and pattern recognition*, pp. 4209–4219, 2024b.
- J Ryan Shue, Eric Ryan Chan, Ryan Po, Zachary Ankner, Jiajun Wu, and Gordon Wetzstein. 3d neural field generation using triplane diffusion. In *Proceedings of the IEEE/CVF Conference on Computer Vision and Pattern Recognition*, pp. 20875–20886, 2023.
- Yawar Siddiqui, Antonio Alliegro, Alexey Artemov, Tatiana Tommasi, Daniele Sirigatti, Vladislav Rosov, Angela Dai, and Matthias Nießner. Meshgpt: Generating triangle meshes with decoderonly transformers. In *Proceedings of the IEEE/CVF conference on computer vision and pattern recognition*, pp. 19615–19625, 2024.
- Ondrej Št'ava, Bedrich Beneš, Radomir Měch, Daniel G Aliaga, and Peter Krištof. Inverse procedural modeling by automatic generation of l-systems. In *Computer graphics forum*, volume 29, pp. 665–674. Wiley Online Library, 2010.
- Jiaxiang Tang, Zhaoshuo Li, Zekun Hao, Xian Liu, Gang Zeng, Ming-Yu Liu, and Qinsheng Zhang. Edgerunner: Auto-regressive auto-encoder for artistic mesh generation. arXiv preprint arXiv:2409.18114, 2024.

- Zhicong Tang, Shuyang Gu, Chunyu Wang, Ting Zhang, Jianmin Bao, Dong Chen, and Baining Guo. Volumediffusion: Flexible text-to-3d generation with efficient volumetric encoder. *arXiv* preprint arXiv:2312.11459, 2023.
- Ashish Vaswani, Noam Shazeer, Niki Parmar, Jakob Uszkoreit, Llion Jones, Aidan N Gomez, Łukasz Kaiser, and Illia Polosukhin. Attention is all you need. *Advances in neural information processing systems*, 30, 2017.
- Fuzhang Wu, Dong-Ming Yan, Weiming Dong, Xiaopeng Zhang, and Peter Wonka. Inverse procedural modeling of facade layouts. *arXiv preprint arXiv:1308.0419*, 2013.
- Jiajun Wu, Chengkai Zhang, Tianfan Xue, William T Freeman, and Joshua B Tenenbaum. Learning a probabilistic latent space of object shapes via 3d generative-adversarial modeling. In *Advances in Neural Information Processing Systems*, pp. 82–90, 2016.
- Jianfeng Xiang, Zelong Lv, Sicheng Xu, Yu Deng, Ruicheng Wang, Bowen Zhang, Dong Chen, Xin Tong, and Jiaolong Yang. Structured 3d latents for scalable and versatile 3d generation. In Proceedings of the Computer Vision and Pattern Recognition Conference, pp. 21469–21480, 2025.
- Jianwen Xie, Yifei Xu, Zilong Zheng, Song-Chun Zhu, and Ying Nian Wu. Generative pointnet: Deep energy-based learning on unordered point sets for 3d generation, reconstruction and classification. In *Proceedings of the IEEE/CVF Conference on Computer Vision and Pattern Recognition*, pp. 14976–14985, 2021.
- Biao Zhang, Jiapeng Tang, Matthias Niessner, and Peter Wonka. 3dshape2vecset: A 3d shape representation for neural fields and generative diffusion models. *ACM Transactions On Graphics* (*TOG*), 42(4):1–16, 2023.
- Susan Zhang, Stephen Roller, Naman Goyal, Mikel Artetxe, Moya Chen, Shuohui Chen, Christopher Dewan, Mona Diab, Xian Li, Xi Victoria Lin, et al. Opt: Open pre-trained transformer language models. *arXiv preprint arXiv:2205.01068*, 2022.
- Wang Zhao, Yan-Pei Cao, Jiale Xu, Yuejiang Dong, and Ying Shan. Di-pcg: Diffusion-based efficient inverse procedural content generation for high-quality 3d asset creation. In *Proceedings of the Computer Vision and Pattern Recognition Conference*, pp. 11061–11072, 2025.
- Linqi Zhou, Yilun Du, and Jiajun Wu. 3d shape generation and completion through point-voxel diffusion. In *Proceedings of the IEEE/CVF international conference on computer vision*, pp. 5826–5835, 2021.

# A APPENDIX

#### A.1 ADDITIONAL QUALITATIVE RESULTS

To further demonstrate the performance of our model, we provide additional qualitative results in Fig. 6 on synthetic data, Fig. 7 and Fig. 8 on real-world images. The synthetic examples highlight the model's ability to reconstruct both global structure and fine-grained geometric details across diverse categories. The real-world examples show that our method generalizes beyond the synthetic training domain, producing structurally consistent and geometrically faithful reconstructions despite the presence of noise, occlusion, and domain shift.

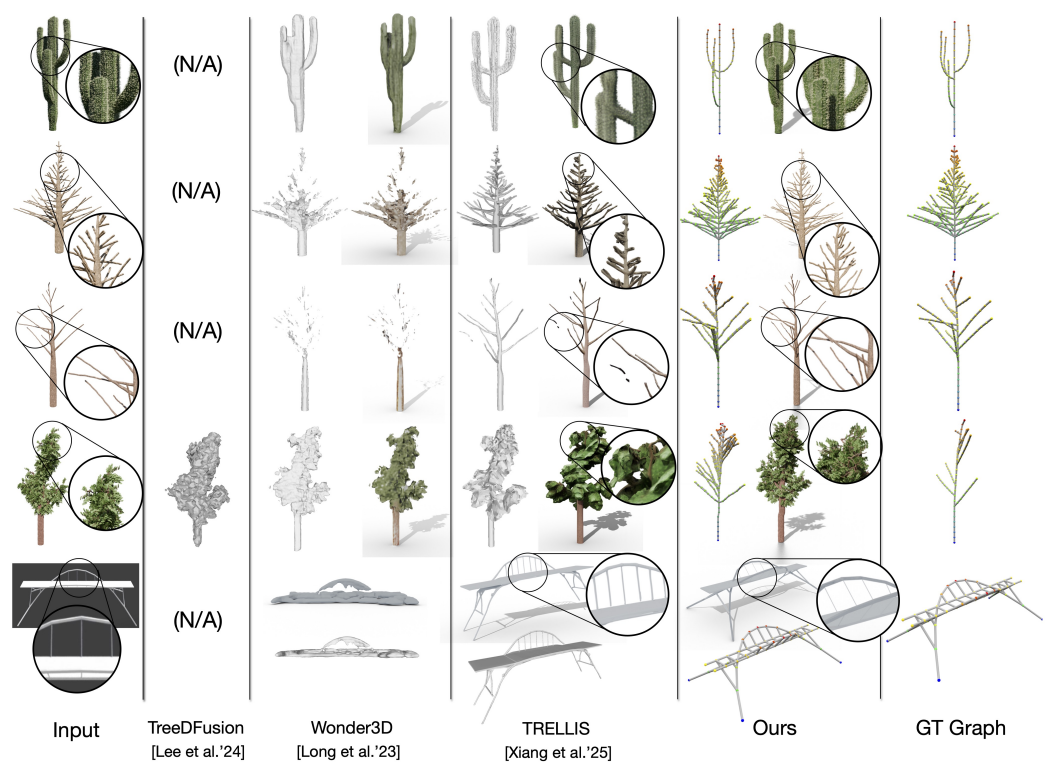


Figure 6: Additional qualitative comparisons with state-of-the-art 3D generative models TRELLIS and Wonder3D. ProcGen3D achieves improved reconstruction quality and consistency with the input images.

#### A.2 DATASET

We construct our dataset with categories of varying complexity in their procedural graphs. Cacti tend to be simpler, with approximately 30–100 vertices in their graphs. Bridge graphs contain 20–140 vertices, while standard trees range from 50–400 vertices. Pine trees are the most complex, with 300–600 vertices. This variation in structural complexity allows us to systematically evaluate the scalability and robustness of our method across both simple and highly complex objects. Based on these procedural graphs, we use the corresponding procedural generators to synthesize full 3D assets with geometry and realistic textures. As illustrated in Fig. 9, our dataset covers diverse categories and structural complexities, providing a challenging benchmark for evaluation.

#### A.3 INFERENCE TIME

Introducing MCTS at inference time improves our reconstruction performance and alignment with the input images, though it comes at the cost of increased inference time, particularly for complex categories with multiple plausible solutions (e.g., tree and pine tree, due to strong self-occlusions), as shown in Tab. 4. To help improve performance, we adopt a dynamic expansion strategy that

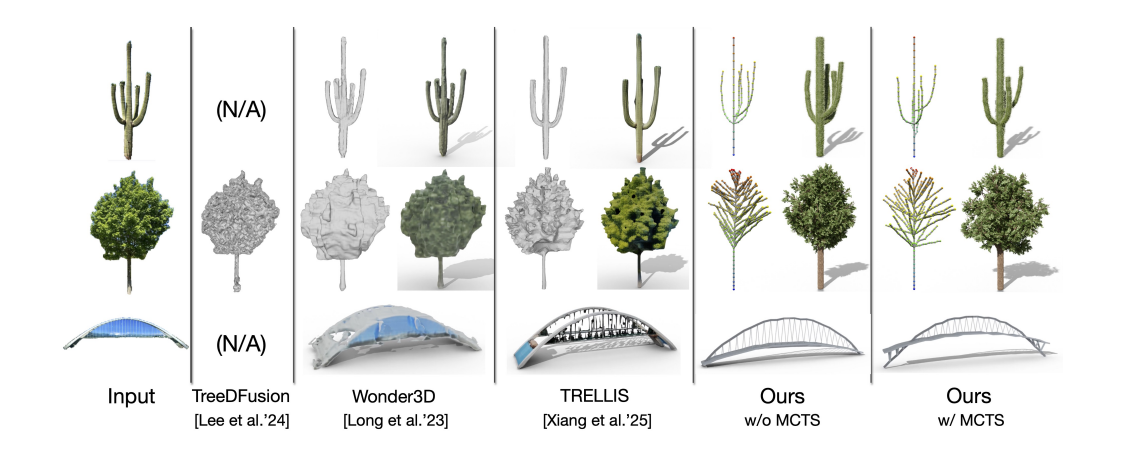


Figure 7: Additional qualitative comparison with state-of-the-art 3D generative models TRELLIS and Wonder3D on real world images. Notably, the cactus and bridge inputs differ significantly from the training data, yet our method is still able to reconstruct objects with similar topology.

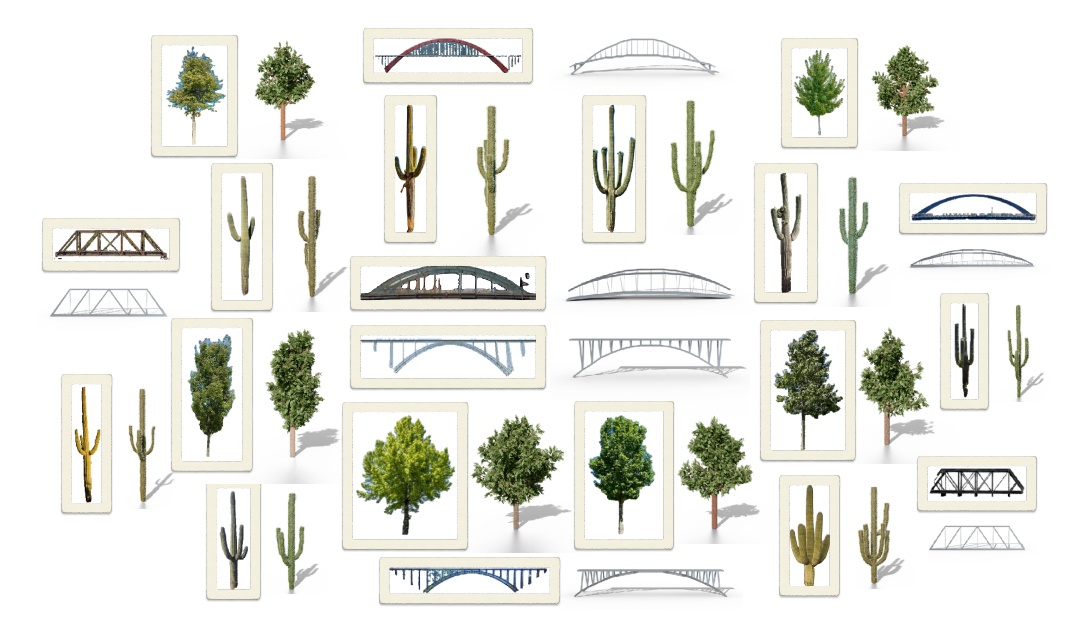


Figure 8: Gallery of real-world reconstructions with procedural graphs. Across a wide variety of inputs, our approach consistently generates high-fidelity 3D reconstructions that are both structurally coherent and geometrically detailed.

adjusts the number of simulations based on the branching factor. Specifically, at each expansion step of the current state, given the predicted logits from the transformer prior, we apply top-k top-p sampling with k=50 and p=0.95 to propose n candidate edges for sequence continuation. If n=1, the child state is selected directly and simulations are skipped. Otherwise, we perform  $n \times ratio$  simulations, where the ratio controls the trade-off between computational cost and search quality. Our approach remains relatively unoptimized for speed, however, and could be substantially accelerated through parallelizing simulations across multiple GPUs or CPUs.

#### A.4 LIMITATIONS

While our ProcGen3D approach demonstrates strong potential as a compact and geometry-faithful representation for 3D content creation, several limitations remain. Since our approach builds on procedural generators for data, we focus on categories where such generators are available. Addition-

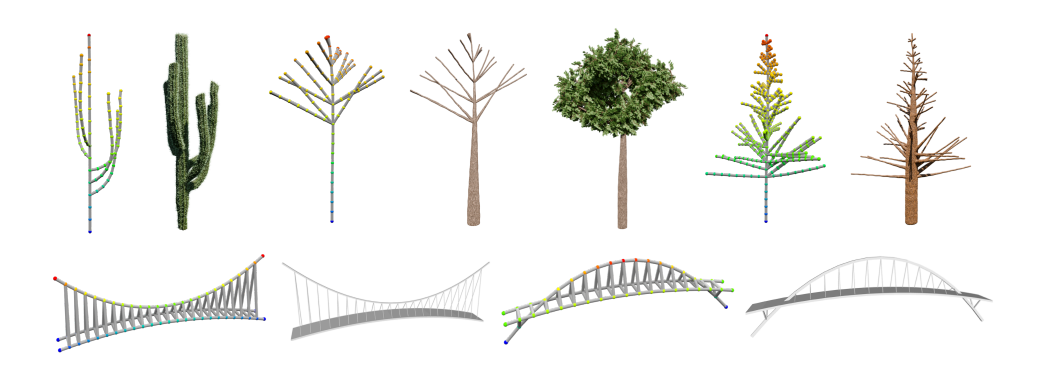


Figure 9: Examples of data samples from our dataset, which inclues cacti, trees, pine trees, and bridges. The dataset spans a wide range of structural complexities, from simple graphs with tens of vertices to highly complex graphs with several hundred vertices.

Table 4: Comparison of the average inference time per sample for conditional generation (w/o MCTS) and MCTS across different categories.

Category	w/o MCTS	w/ MCTS
Cactus	11s	<1min
Tree	24s	24min
Pinetree	48s	42min
Bridge	31s	2min

ally, while our MCTS-guided sampling improves consistency with input images, it also introduces additional computational cost compared to conditional feedforward generation only.